

# Variable stars in young open star cluster NGC 7380

Sneh Lata<sup>1\*</sup>, A. K. Pandey<sup>1</sup>, Neelam Panwar<sup>2</sup>, W. P. Chen<sup>3</sup>

M. R. Samal<sup>4</sup>, J. C. Pandey<sup>1</sup>

<sup>1</sup>*Aryabhata Research Institute of Observational Sciences, Manora Peak, Nainital 263002, Uttarakhand, India*

<sup>2</sup>*Department of Physics & Astrophysics, University of Delhi-110007, India*

<sup>3</sup>*Institute of Astronomy, National Central University, 300 Jhongda Rd, Jhongli, Taoyuan Country 32054, Taiwan*

<sup>4</sup>*Aix-Marseille Université, CNRS, Laboratoire d'Astrophysique de Marseille UMR 7326, 13388, Marseille, France*

Accepted ———. Received ———;

## ABSTRACT

We present time series photometry of 57 variable stars in the cluster region NGC 7380. The association of these variable stars to the cluster NGC 7380 has been established on the basis of two colour diagrams and colour-magnitude diagrams. Seventeen stars are found to be main-sequence variables, which are mainly B type stars and are classified as slowly pulsating B stars,  $\beta$  Cep or  $\delta$  Scuti stars. Some of them may belong to new class variables as discussed by Mowlavi et al. (2013) and Lata et al. (2014). Present sample also contains 14 pre-main-sequence stars, whose ages and masses are found to be mostly  $\lesssim 5$  Myr and range  $0.60 \lesssim M/M_{\odot} \lesssim 2.30$  and hence should be T-Tauri stars. About half of the weak line T-Tauri stars are found to be fast rotators with a period of  $\lesssim 2$  days as compared to the classical T-Tauri stars. Some of the variables belong to the field star population.

**Key words:** Open cluster: NGC 7380 – colour-magnitude diagram: Variables: pre-main sequence stars

## 1 INTRODUCTION

NGC 7380 (RA=22h 47m 21s, Dec +58° 07' 54'') is a young open cluster in the northern sky. Several studies of the NGC 7380 region based on photometric observations have already been carried out (e.g., Moffat 1971; Chen et al. 2011 and references therein). The members of the cluster were identified by Baade (1983) on the basis of photometric observations by Moffat (1971). They identified a few T-Tauri stars (TTs) and Herbig Ae stars in the region. Mathew et al. (2010, 2012) found a number of pre-main-sequence (PMS) stars on the basis of optical and near IR photometry. Chen et al. (2011) have carried out a detailed study of the region. Using the proper motion data they identified probable members of the cluster. They found that the reddening towards the direction of the cluster is variable with  $E(B-V)_{min}=0.5$  mag and  $E(B-V)_{max}=0.7$  mag and the cluster is located at a distance of  $2.6 \pm 0.4$  kpc. Using surface density map of 2MASS stars, Chen et al. (2011) also found that the cluster is elongated in the north-south direction with an average angular radius of 4 arcmin which corresponds to 3 pc at the distance of the cluster. They estimated the age of the

cluster as  $\sim 4$  Myr. The O-type binary star DH Cep is a member of the cluster which is in its late stage of clearing the surrounding material, and may have triggered the ongoing star formation in neighbouring molecular clouds which harbour young stars that are coeval and comoving but not gravitationally bound. This cluster has been an interesting and important object because it contains a massive binary system DH Cep (=HD 215835;  $V = 8.58$ ) which is a double-lined, massive spectroscopic binary having a pair of O5-6 V stars with an orbital period of 2.111 days (Lines et al. 1986; Semeniuk 1991; Pearce 1949). This star is located at the center of the cluster and found to be an ionizing star for the emission nebula (Underhill 1969). Underhill (1969) found a very high fraction of binaries in the region. Of the 10 stars observed by Underhill (1969), 6 are detected and 4 are suspected spectroscopic binaries.

We find NGC 7380 an interesting object as it is an extremely young open cluster which contains several PMS stars, massive stars O/B type stars as well as other main-sequence (MS) stars. Therefore we carried out photometric observations of the NGC 7380 region to search for variable stars. Photometric variability in OB supergiants, early B-type stars, Be stars, mid to late B-type stars occurs mostly due to the pulsations (Stankov & Handler 2005; Kiriakidis

\* E-mail: sneh@aries.res.in

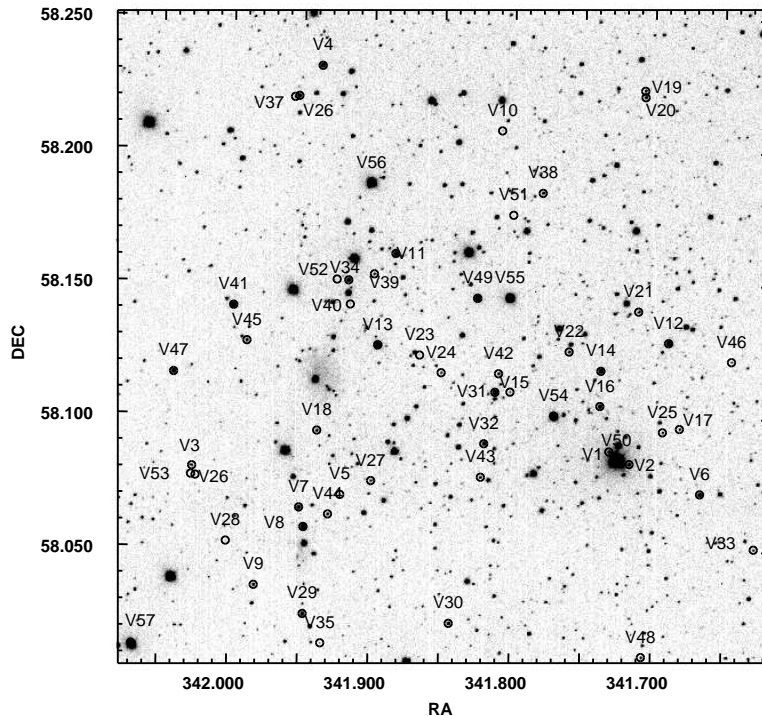


**Figure 1.** The observed region of NGC 7380 in V band. The variable candidates detected in the present work are encircled and labeled with numbers. The epoch of equatorial coordinates RA and DEC is J2000.0.

et al. 1992; Moskalik & Dziembowski 1992). Pulsating variable stars expand and contract in a repeating cycle of size changes. The different types of pulsating variables are distinguished by their periods of pulsation and the shapes of their light curves. In PMS objects like TTSs (mass  $\lesssim 3 M_{\odot}$ ) photometric variations are believed to originate from several mechanisms like rotation of a star with an asymmetrical distribution of cool spots, variable hot spots or obscuration by circumstellar dust (see Herbst et al. 1994 and reference therein). The Herbig Ae/Be stars (PMS stars having mass  $\gtrsim 3 M_{\odot}$ ) also show variability as they move across the instability region in the Hertzsprung-Russell (HR) diagram on their way to the MS. Several systematic studies of TTSs have been carried out which revealed different type of variabilities (Herbst et al. 1994). It is now well known that some of PMS stars show periodic variability (e.g., Hillenbrand 2002; Schaefer 1983; Bouvier et al. 1993; Bouvier 1994; Percy et al. 2006, 2010).

NGC 7380 has been monitored on 70 nights during October 2012 to February 2013 to identify and characterize the variable stars in the region. In Section 2 we describe the observations, data reduction procedure, variable identification and period determination. In Section 3 we discuss association of the detected variables with the cluster using  $(U - B)/(B - V)$  and  $(J - H)/(H - K)$  two colour diagrams (TCDs) and the  $V/(V - I)$  colour-magnitude diagram (CMD). Section 4 describes the age and mass estimation of young stellar objects. In Section 5 we study the spectral energy distribution of identified young stellar objects. Sec-

tion 6 describes luminosity and temperature of the stars. We characterize variable stars in Section 7. In section 8 we studied the effect of NIR excess on the rotation, whereas section 9 discusses the correlation among rotation, mass, age and amplitude. We summarise our results in Section 10.

## 2 OBSERVATIONS AND DATA REDUCTION

The photometric observations of NGC 7380 were taken using the 0.81-m f/7 Ritchey-Chretien Tenagara automated telescope in southern Arizona. The telescope has a  $1024 \times 1024$  pixel SITE camera. Each pixel corresponds to 0.87 arcsec which yields a field of view of  $\sim 14.8 \times 14.8$  arcmin<sup>2</sup>. The observations were taken in V and I filters during 2012 October 19 to 2013 February 08 on 70 nights. Each night consists of 2 to 4 frames in V and I filters. On two nights 23 November 2012 and 24 November 2012 each had around 150 observations. The typical seeing (estimated from full width at half maximum of the point like stars) of the images was  $\sim 2$  to  $\sim 3$  arcsec. Bias and twilight flats were also taken along with the target field. The observed region is shown in Fig. 1.

The preprocessing of the CCD images was performed using the IRAF<sup>1</sup> and the instrumental magnitude of the

<sup>1</sup> IRAF is distributed by the National Optical Astronomy Observatory, which is operated by the Association of Universities for Research in Astronomy (AURA) under cooperative agreement with the National Science Foundation.

stars were obtained using the DAOPHOT package (Stetson 1987). Details can be found in our earlier papers (Lata et al. 2011, 2012). We have used the DAOMATCH (Stetson 1992) routine of DAOPHOT to find the translation, rotation and scaling solutions between different photometry files, whereas DAOMASTER (Stetson 1992) matches the point sources. To remove frame-to-frame flux variation due to airmass and exposure time, we used DAOMASTER programme to get the corrected magnitude. This task makes the mean flux level of each frame equal to the reference frame by an additive constant. The first target frame taken on 23 November 2012 has been considered as the reference frame. Present observations have 641 and 631 frames in the  $V$  and  $I$  band respectively and each frame corresponds to one photometry file. We have considered only those stars for further study which have at least 100 observations in the  $V$  and  $I$ . From the output of DAOMASTER, we get corrected magnitudes listed in a `.cor` file. This file is further used to search for variable stars in the next section.

The standardization of the stars in the cluster field was carried out with the help of the data given by Chen et al. (2011). The instrumental magnitudes were transformed to the standard Johnson  $V$  and Cousins  $I$  system. The equations used for photometric calibration are given below:

$$V - v = (-0.001 \pm 0.002) \times (V - I) + (0.902 \pm 0.007)$$

$$V - I = (0.965 \pm 0.011) \times (v - i) + (1.201 \pm 0.006)$$

Where  $V$  and  $I$  are standard magnitude of stars and  $v$  and  $i$  are instrumental magnitudes of stars in  $V$  and  $I$  filters. The mean value of the photometric error of the data was estimated using the observations of each star. The mean error as a function of instrumental magnitude is shown in Fig. 2. The mean error is found to be  $\sim 0.01$  mag at magnitude  $\leq 13$  mag and increases to  $\sim 0.1$  mag at  $\sim 17$  mag.

## 2.1 Variable identification and period determination

The differential magnitudes ( $\Delta m$ ) of stars in the sense variable minus comparison star were plotted against Julian date (JD). The probable variables were identified visually by inspecting the light curves. The visual inspection yields 57 variable candidates, of which 50 were detected in  $V$  band and 54 in  $I$  band including the massive binary DH Cep (HD 215835). The brightness of these variables vary from short to long time scale periods. The samples of short and long period variables are shown in Figs. 3 and 4, respectively.

The identification number, coordinates and present  $VI$  photometric data for these variable stars are given in Table 1. The CCD pixel coordinates of these identified variables were converted to celestial coordinates (RA and DEC) for J2000 with the help of the CCMAP and CCTRAN tasks in IRAF.

The variability of stars nos 51 to 57 could only be detected in  $I$  band. Stars no 54, 55, 56 and 57 got saturated in  $V$  band. Star no 51 to 53 are too faint to detect in  $V$  band. Similarly, variability for stars 23, 28 and 35 could not be detected in  $I$  band. Table 1 also lists  $NIR$  data taken from the 2MASS catalogue (Cutri et al. 2003). The variable

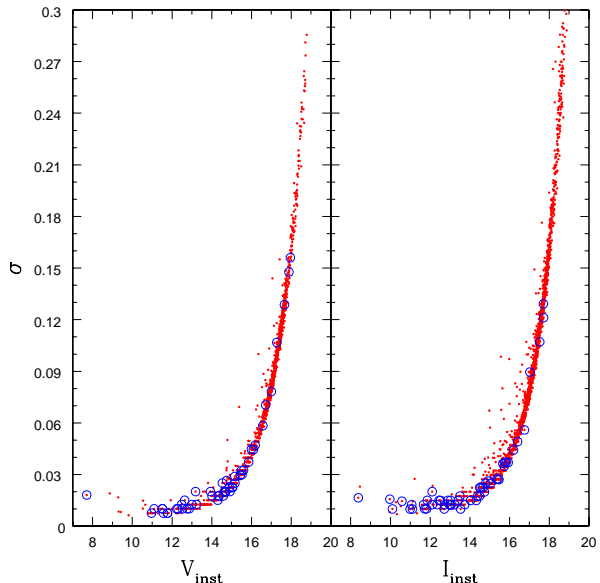


**Figure 2.** Mean photometric errors given by DAOPHOT as a function of magnitude in  $V$  and  $I$ . Open circles represent variable candidates.

candidates identified in the present work are marked in Fig. 1.

In order to determine the probable periods of the variable stars we used the Lomb-Scargle (LS) periodogram (Lomb 1976; Scargle 1982). This method works well with unevenly sampled data. We used the algorithm available at the Starlink<sup>3</sup> software database. We further confirmed the periods using NASA exoplanet archive periodogram service. We visually inspected the phased light curves and opted the period showing the best light curve. The most probable periods with amplitude are listed in Table 1. The light curves of variable stars are folded with their estimated periods. The phased light curves will be discussed in Section 5.

## 3 ASSOCIATION OF YOUNG STELLAR OBJECTS (YSOs) WITH THE CLUSTER

To understand the nature of the variable candidates it is necessary to find out their association to the cluster NGC 7380. The  $U - B/B - V$  and  $J - H/H - K$  TCDs,  $V/V - I$  CMD have been used to find out the association of the identified variables with NGC 7380 region. In addition, we have also used proper motion data from Chen et al. (2011) listed in Table 2 as well as X-ray data listed in Table 3 to identify the PMS variables associated with NGC 7380 region.

Since PMS stars (both classical TTSs and weak-line TTSs) are strong X-ray emitters, the X-ray observations of PMS stars play an important role in identification of PMS stars associated with star forming regions (see e.g., Pandey et al 2014). In fact, the level of X-ray emission in the PMS stars, which is higher than that of MS stars, provides a very efficient mean of selecting PMS stars. However,

<sup>3</sup> <http://www.starlink.uk>

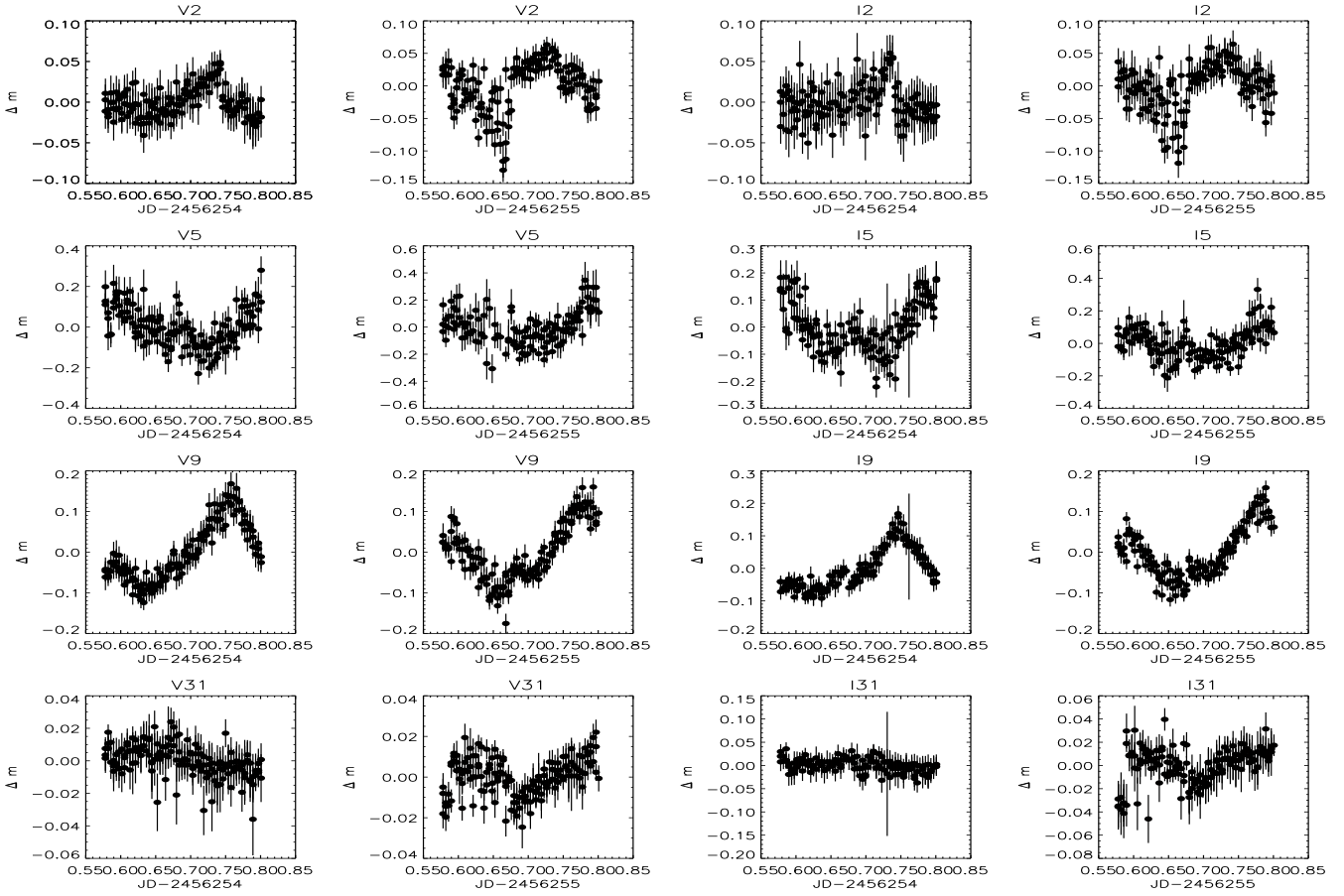


**Figure 3.** The light curves of a few short period variable stars in *V* and *I* band identified in the present work. The ID e.g., V2 and I2 represent variable no 2 in *V* and *I* bands, respectively. The  $\Delta m$  represents the differential magnitude.

**Table 2.** Proper motion data taken from Chen et al. (2011).

id	$\mu_{RA}$ (SHAO) (mas/yr)	$\mu_{DEC}$ (SHAO) (mas/yr)	$\mu_{RA}$ (UCAC3) (mas/yr)	$\mu_{DEC}$ (UCAC3) (mas/yr)
4	$-3.309 \pm 0.484$	$-3.049 \pm 1.056$	$-8.1 \pm 1.0$	$-7.6 \pm 1.5$
6	$3.253 \pm 0.730$	$-1.002 \pm 1.314$	$0.2 \pm 2.3$	$-10.3 \pm 4.6$
7	$5.610 \pm 1.025$	$-1.575 \pm 1.304$	$-5.7 \pm 2.7$	$1.2 \pm 5.9$
8	$2.731 \pm 0.532$	$-0.508 \pm 1.787$	$2.0 \pm 3.4$	$-4.7 \pm 11.1$
11	$1.084 \pm 0.405$	$0.259 \pm 1.445$	$-2.8 \pm 1.2$	$-3.1 \pm 2.2$
12	$1.070 \pm 0.433$	$-0.877 \pm 1.055$	$-0.5 \pm 3.3$	$-4.1 \pm 1.9$
13	$-0.287 \pm 0.382$	$-1.353 \pm 1.415$	$-3.1 \pm 0.8$	$-3.8 \pm 0.9$
14	$0.816 \pm 0.415$	$-3.521 \pm 0.682$	$-2.8 \pm 1.0$	$-3.3 \pm 1.8$
29	$-14.553 \pm 0.532$	$-14.721 \pm 1.050$	$-20.4 \pm 2.7$	$-15.7 \pm 3.1$
31	$0.848 \pm 0.373$	$-2.625 \pm 0.789$	$-3.6 \pm 2.1$	$-4.1 \pm 1.1$
32	$2.735 \pm 0.583$	$-7.836 \pm 1.718$	$-6.5 \pm 2.0$	$-5.0 \pm 6.1$
34	$-1.160 \pm 0.641$	$-6.407 \pm 1.499$	$-3.5 \pm 2.0$	$-4.6 \pm 6.2$
36	$12.446 \pm 0.607$	$-1.615 \pm 1.890$	$9.2 \pm 2.6$	$-4.9 \pm 4.1$
41	$2.392 \pm 0.726$	$-3.801 \pm 1.583$	$-1.6 \pm 2.0$	$-0.7 \pm 1.8$
47	$-2.893 \pm 0.655$	$-3.094 \pm 1.961$	$-3.9 \pm 1.4$	$-2.6 \pm 4.6$
49	$1.278 \pm 0.426$	$-1.676 \pm 1.181$	$-2.4 \pm 0.6$	$-3.6 \pm 0.7$
50	$-4.11 \pm 1.290$	$-2.80 \pm 1.190$	$-2.7$	$-3.6$
54	$-0.342 \pm 0.692$	$-1.161 \pm 0.813$	$-2.3 \pm 0.8$	$-3.5 \pm 0.8$
55	$0.292 \pm 0.417$	$-1.658 \pm 1.848$	$-1.8 \pm 0.6$	$-2.9 \pm 0.6$

the origin of X-ray emission from PMS low mass stars is still poorly understood. In massive stars, the X-ray emission arises from shocks in radiatively-driven winds (Lucy & White 1980; Owocki & Cohen 1999; Kudritzki & Puls 2000; Crowther 2007), while in the low-mass stars, rotation with

**Table 3.** X-ray data.

id	PNf	Mf	Avef
7	9.36	10.08	9.72
13	3.98	4.79	4.39
15	1.58	1.36	1.47
27	2.54	1.57	2.06
30	3.5	3.72	3.61
50	83.9	80.65	82.28
53	22.94	28.46	25.7

PNf: flux from PN detector in units of  $10^{-14}$  erg/s/cm<sup>2</sup>

Mf: flux from MOS detector in units of  $10^{-14}$  erg/s/cm<sup>2</sup>

Avef: Average flux from PN and MOS detector in units of  $10^{-14}$  erg/s/cm<sup>2</sup>

convective envelopes drives a magnetic dynamo leading to strong X-ray emission (Vaiana et al. 1981; Güdel 2004). Intermediate mass stars, on the other hand, are expected to be X-ray dark because (a) the wind is not strong enough to produce X-rays as in the case of massive stars (see Lucy & White 1980; Kudritzki & Puls 2000), and (b) being fully radiative internal structure, the dynamo action cannot support the X-ray emission.

The X-ray data for the NGC 7380 region have been taken from Bhatt et al. (2010, 2013). They have analyzed archival X-ray data from XMM-Newton observations for the region containing NGC 7380. Data were acquired simultaneously with EPIC-PN camera (Strüder et al. 2001) and two

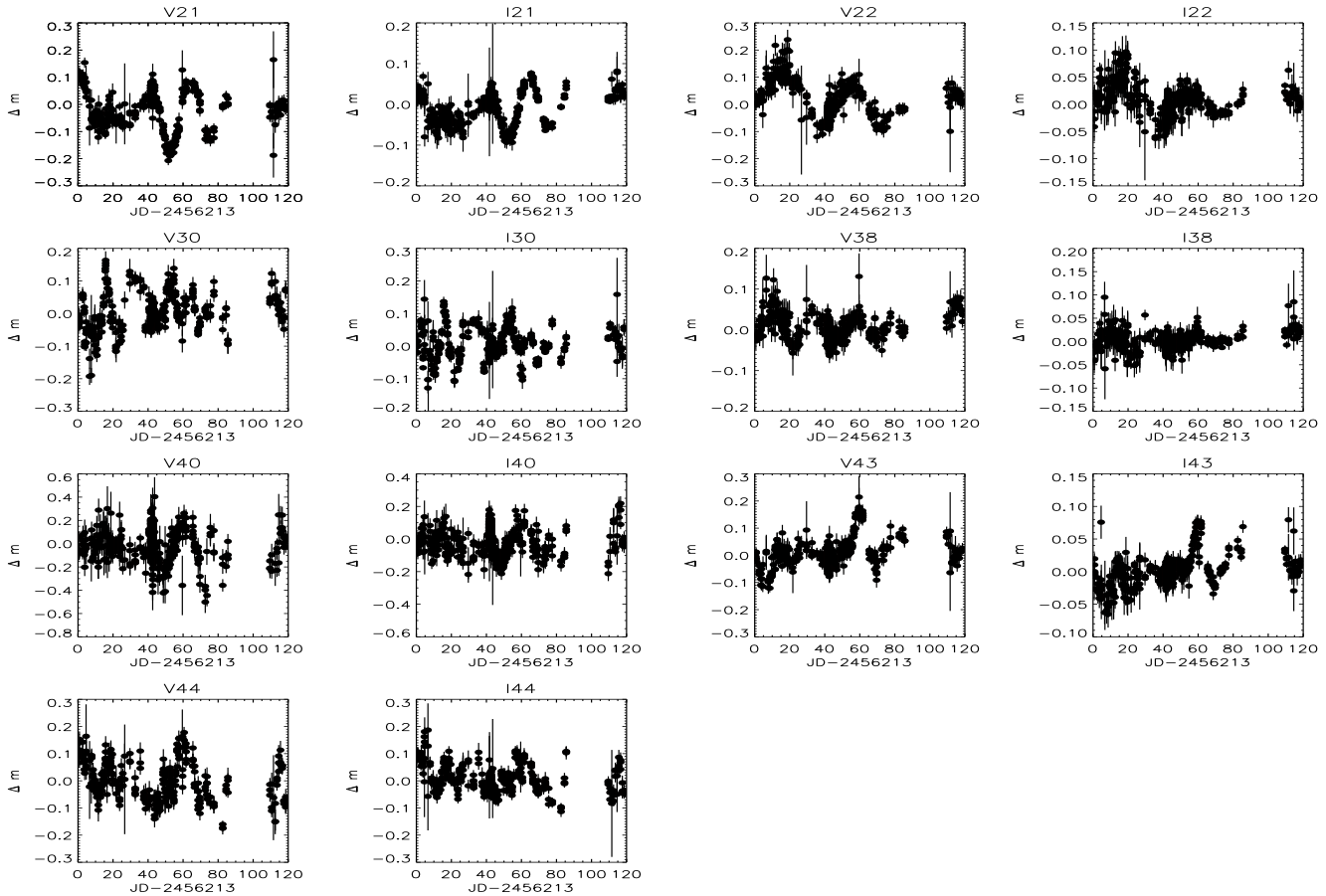


**Figure 4.** The light curves of a few long period variable stars identified in the present work, each with 70 nights observations. The  $\Delta m$  represents the differential magnitude.

nearly identical EPIC-MOS (MOS1 and MOS2; Turner et al. 2001) cameras. We identified the X-ray data for seven variable stars namely 7, 13, 15, 27, 30, 50 (DH cep) and 53. The matching radius was 6 arcsec.

To establish membership further we used proper motion data of stars in NGC 7380 from Chen et al. (2011). Out of 57 stars only 18 stars have proper motion data. Table 2 lists two data sets of proper motions and associated errors from UCAC3 and SHAO. Typical errors in proper motions range from 1 to 10 mas/yr for UCAC3, and  $< 1$  mas/yr for the SHAO. The mean proper motion for NGC 7380 has been determined as  $\mu_{RA} = -1.74 \pm 0.84$  and  $\mu_{DEC} = -2.52 \pm 0.81$  by Baumgardt et al. (2000). The proper motion values of the present sample except star nos 7, 29, 32 and 36 are within  $3\sigma$  limit. Thus proper motion data suggest that star nos 7, 29, 32 and 36 could be non-members.

In the absence of kinematical data of the remaining stars we have used photometric data to determine their membership to the cluster. We have used  $(U - B)/(B - V)$  and  $(J - H)/(H - K)$  TCDs and  $V/V - I$  CMD to find out the probable member stars associated with the NGC 7380 region.

### 3.1 $(U - B)/(B - V)$ and $(J - H)/(H - K)$ TCDs

Fig. 5 shows  $(U - B)/(B - V)$  TCD for the variable candidates. The  $UBV$  data have been taken from Chen et al. (2011) and WEBDA. Out of 53 variable candidates  $UBV$  data are available for 33 stars and these are plotted in  $(U - B)/(B - V)$  TCD. The distribution of variables in Fig. 5 reveals a variable reddening in the cluster region. The identification of young stellar objects (YSOs) or estimation of reddening for YSOs is not possible using the  $(U - B)/(B - V)$  TCD because the  $U$  and  $B$  band fluxes may be affected by excess due to accretion. The sources lying near the MS with O to A spectral type are considered as MS type stars.

The young stellar objects (YSOs) are easily recognized by their  $H\alpha$  emission, NIR excess, or X-ray emission, therefore  $(J - H)/(H - K)$  TCD is one of the very useful tools to identify PMS objects. Fig. 6 shows the  $(J - H)/(H - K)$  TCD for variable stars. We have used  $JHK$  data from the 2MASS catalogue (Cutri et al. 2013) and converted to CIT system using the relations given in the 2MASS website (<http://www.astro.caltech.edu/~jmc/2mass/v3/transformations/>).

The solid and long dashed lines in Fig. 6 represents unreddened MS and giant locus (Bessell & Brett 1988) respectively. The dotted line indicates the intrinsic locus of CTTSs (Meyer et al. 1997). The parallel dashed lines are the reddening vectors drawn from the tip (spectral type M4) of the giant branch ('left reddening line'), from the base

**Table 1.** The present photometric data, NIR data, period and amplitude of 57 variables in the region of NGC 7384. The NIR data have been taken from 2MASS point source catalogue (Cutri et al. 2003).

ID	$\alpha_{2000}$ degree	$\delta_{2000}$ degree	$V - I$ mag	$V$ mag	$J$ mag	$H$ mag	$K$ mag	[period] day	[Amp.] mag
1	341.730639	58.087500	0.682±0.036	16.079±0.029	14.949±0.041	14.504±0.05	14.467±0.087	0.167	0.108
2	341.716194	58.082861	0.603±0.022	14.847±0.020	13.725±0.029	13.607±0.033	13.576±0.044	0.198	0.027
3	342.026556	58.080361	1.994±0.022	16.442±0.032	12.550±0.031	11.843±0.048	11.597±0.041	1.151	0.100
4	341.937500	58.231500	0.798±0.012	13.226±0.010	11.770±0.022	11.534±0.029	11.422±0.021	4.729	0.146
5	341.921167	58.070111	1.391±0.049	17.652±0.058	14.978±0.037	14.480±0.054	14.382±0.08	0.325	0.120
6	341.665917	58.071778	1.033±0.010	13.440±0.010	11.637±0.023	11.330±0.03	11.258±0.023	1.255	0.015
7	341.950222	58.065167	0.959±0.017	14.144±0.013	12.253±0.03	11.879±0.036	11.730±0.031	0.249	0.015
8	341.946917	58.057806	1.602±0.009	12.428±0.010	9.580±0.023	8.894±0.023	8.794±0.021	0.143	0.015
9	341.981556	58.035750	1.241±0.022	15.372±0.025	13.355±0.027	12.905±0.032	12.835±0.035	0.259	0.076
10	341.809000	58.207806	1.422±0.089	18.126±0.106	15.628±0.072	15.223±0.082	14.922±0.134	0.234	0.160
11	341.883778	58.161111	0.563±0.015	12.674±0.008	11.652±0.023	11.567±0.028	11.480±0.021	1.074	0.012
12	341.689111	58.128528	0.728±0.020	12.464±0.008	11.105±0.032	10.898±0.042	10.666±0.032	1.423	0.018
13	341.895778	58.126639	0.531±0.012	11.857±0.007	10.989±0.02	10.892±0.033	10.851±0.029	1.235	0.016
14	341.736972	58.117806	0.562±0.015	13.143±0.010	12.125±0.028	12.021±0.035	11.897±0.028	5.463	0.014
15	341.801389	58.109528	1.465±0.037	16.999±0.044	14.196±0.034	13.604±0.038	13.471±0.042	9.720	0.059
16	341.737417	58.104556	0.659±0.014	13.774±0.010	12.562±0.023	12.429±0.032	12.347±0.028	0.406	0.011
17	341.680750	58.096278	1.876±0.017	15.996±0.022	12.603±0.023	11.802±0.028	11.555±0.021	0.067	0.023
18	341.938194	58.094194	1.270±0.024	15.759±0.022	13.246±0.029	12.772±0.036	12.564±0.03	2.552	0.036
19	341.707417	58.223417	1.794±0.014	15.534±0.020	12.294±0.024	11.586±0.03	11.389±0.025	3.300	0.028
20	341.707139	58.221000	1.775±0.012	15.242±0.018	11.988±0.024	11.337±0.03	11.077±0.023	0.767	0.027
21	341.710583	58.140278	0.499±0.010	15.614±0.020	8.644±0.019	7.563±0.033	7.135±0.021	1.050/20.71	0.068
22	341.759722	58.124917	3.678±0.012	15.560±0.020	9.351±0.023	8.180±0.038	7.743±0.016	48.879/1.02	0.058
23	341.865917	58.123000	-	18.463±0.128	15.767±0.09	15.421±0.148	14.541	0.050	0.189
24	341.850444	58.116472	0.981±0.034	16.470±0.030	14.385±0.039	14.165±0.044	14.008±0.066	0.073	0.044
25	341.692778	58.094972	2.050±0.019	16.490±0.032	12.756±0.023	11.897±0.03	11.638±0.019	0.134	0.046
26	342.024056	58.076861	0.887±0.129	18.334±0.147	16.334±0.127	15.748±0.152	13.953	0.217	0.205
27	341.899417	58.075500	1.579±0.027	16.713±0.037	13.794±0.051	13.115±0.056	12.893±0.046	1.642	0.074
28	342.001861	58.052222	1.435±0.120	18.912±0.156	16.374±0.118	15.956±0.171	15.728±0.3	0.431	0.202
29	341.946583	58.025083	0.842±0.015	13.568±0.015	12.139±0.025	11.805±0.03	11.786±0.025	0.376	0.022
30	341.842972	58.022194	2.129±0.012	14.895±0.016	10.797±0.031	9.763±0.03	8.847±0.021	19.109	0.049
31	341.812083	58.109389	0.472±0.015	12.673±0.008	11.851±0.025	11.761±0.028	11.766±0.025	0.197	0.012
32	341.819500	58.089972	0.839±0.009	14.064±0.020	12.506±0.026	12.344±0.032	12.221±0.026	0.254	0.032
33	341.627417	58.051194	1.345±0.037	16.825±0.045	14.41±0.041	14.013±0.052	13.750±0.059	0.568	0.106
34	341.917028	58.150917	0.976±0.012	13.678±0.010	11.846±0.023	11.505±0.026	11.217±0.023	0.639	0.018
35	341.933778	58.014139	1.430±0.045	17.615±0.070	15.171±0.049	14.836±0.074	14.703±0.112	39.240	0.087
36	341.953778	58.220056	0.969±0.012	13.907±0.010	12.247±0.03	11.815±0.036	11.729±0.029	0.197	0.010
37	341.956833	58.219639	1.196±0.027	16.353±0.029	14.241±0.039	13.908±0.05	13.761±0.056	0.334	0.030
38	341.779528	58.184500	3.140±0.012	15.245±0.017	9.769±0.023	8.674±0.031	8.256±0.023	24.676/1.039	0.029
39	341.898806	58.153333	0.884±0.027	15.892±0.022	14.157±0.035	13.319±0.038	12.238±0.028	48.557	0.038
40	341.915639	58.141833	2.139±0.044	17.966±0.078	14.092±0.035	12.948±0.032	12.169±0.029	21.607	0.133
41	341.998556	58.141056	1.725±0.009	12.434±0.010	9.293±0.023	8.571±0.031	8.360±0.02	0.125	0.008
42	341.809667	58.116389	0.743±0.024	15.506±0.017	13.761±0.025	13.051±0.032	12.252±0.025	60.543	0.026
43	341.821583	58.077361	4.215±0.010	15.829±0.020	8.687±0.026	7.592±0.031	7.121±0.021	11.924	0.031
44	341.929639	58.062694	1.865±0.017	16.073±0.025	12.642±0.025	12.060±0.028	11.727±0.024	30.897/1.029	0.070
45	341.988722	58.127778	1.190±0.014	15.193±0.015	13.186±0.027	12.613±0.031	12.540±0.031	16.423	0.016
46	341.644250	58.121667	1.357±0.037	17.043±0.047	14.349±0.032	13.463±0.033	12.799±0.029	5.586/45.572	0.059
47	342.040500	58.115694	0.724±0.012	13.388±0.012	12.042±0.021	11.865±0.027	11.764±0.024	0.544	0.017
48	341.706528	58.010278	1.028±0.026	15.627±0.026	13.837±0.028	13.439±0.033	13.327±0.037	15.467	0.029
49	341.825194	58.144667	0.488±0.015	11.989±0.010	11.191±0.023	11.092±0.027	11.086±0.02	0.166	0.015
50	341.725167	58.084167	0.580±0.016	8.629±0.018	7.741±0.027	7.718±0.055	7.682±0.016	1.057	0.052
51	341.800278	58.176111	2.060±0.256	19.215±0.318	15.866±0.078	14.900±0.064	14.609±0.096	46.365	0.325
52	341.925278	58.151139	-	-	15.306±0.081	14.231±0.072	13.630±0.059	16.845	0.343
53	342.027278	58.077194	2.320±0.054	17.957±0.128	13.978±0.062	12.636±0.062	11.651±0.039	53.644	0.372
54	341.770194	58.100722	0.529±0.007	11.296±0.006	10.366±0.024	10.236±0.03	10.050±0.021	7.715	0.019
55	341.802167	58.144944	0.381±0.010	10.656±0.014	10.005±0.023	10.005±0.027	9.996±0.02	0.143	0.029
56	341.901778	58.187639	0.523±0.006	10.354±0.007	9.421±0.022	9.197±0.028	9.180±0.02	0.394	0.020
57	342.067833	58.013167	0.709±0.007	10.404±0.007	9.140±0.022	8.976±0.028	8.876±0.02	0.200	0.079

(spectral type A0) of the MS branch ('middle reddening line') and from the tip of the intrinsic Classical T Tauri Stars line ('right reddening line'). The extinction ratios  $A_J/A_V = 0.265$ ,  $A_H/A_V = 0.155$  and  $A_K/A_V = 0.090$  have been adopted from Cohen et al. (1981). The sources lying in 'F' region could be either field stars (MS stars, giants), Class III or Class II sources with small NIR excesses. The sources lying in the 'T' region e.g. 30, 40, 46 and 53 are considered to be mostly CTTs (Class II objects). Majority of the variable candidates are found to be distributed below the intrinsic locus of CTTs and these should be B type MS stars. The stars numbered 3, 10, 20, 21, 27, 41, 43 and 52 located in the 'F' region and lie above the extension of CTTs locus could be the WTTs (Class III sources).

### 3.2 $V/V - I$ colour-magnitude diagram

$V/V - I$  CMD is also an additional tool to identify probable member of the cluster. Fig. 7 shows the  $V/V - I$  CMD for all the identified variables in the region. The filled circles and triangles represent probable CTTs and WTTs, respectively, whereas filled squares and open squares represent MS population in the cluster region and field popu-

lation towards the cluster region, respectively identified on the basis of  $U - B/B - V$  and  $J - H/H - K$  TCDs. In Fig. 7 we have also plotted theoretical isochrone for 4 Myr for  $Z=0.02$  (continuous line) by Girardi et al. (2002) and PMS isochrones for various ages and evolutionary tracks for various masses by Siess et al. (2000). All the isochrones and evolutionary tracks are corrected for the distance (2.6 kpc) and minimum reddening  $E(V - I)=0.625$  mag. The minimum value of  $E(V - I)$  has been estimated using the relation  $E(V - I)/E(B - V) = 1.25$  and  $E(B - V) = 0.50$  mag.

The association of variables to the cluster NGC 7380 is marked 'yes' on the basis of above criteria as well as classification of variables is marked in Table 4. The variables not associated to the cluster is marked 'no' in Table 4.

### 3.3 Field star contamination

To estimate the field star contribution towards the direction of the cluster NGC 7380 we generated star counts in  $1 \times 1$  degree<sup>2</sup> field using the Besancon Galactic model of stellar population synthesis (Robin et al. 2003). The distance to the cluster and  $E(B - V)$  has been taken as 2.6 kpc and 0.5-0.7 mag respectively. The model simulations with dis-



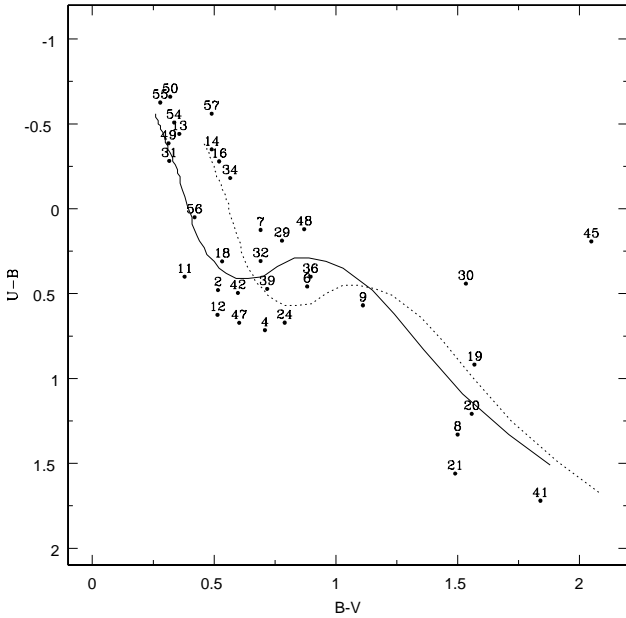


**Figure 5.**  $U-B/B-V$  two colour diagram for identified variable stars. The  $UBV$  data have been taken from Chen et al. (2011). The solid curve represents the zero-age-main-sequence (ZAMS) by Girardi et al. (2002) shifted along the reddening vector of 0.72 for  $E(B-V) = 0.5$  mag and  $E(B-V) = 0.7$  mag.

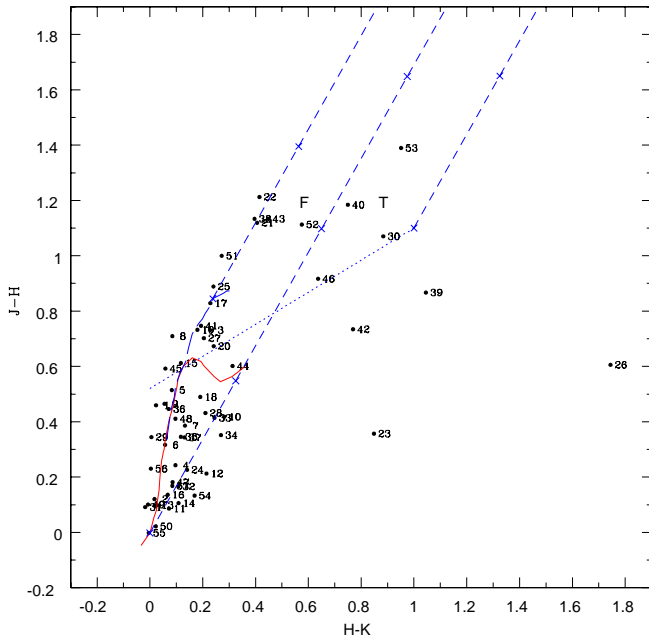


**Figure 6.**  $(J-H/H-K)$  TCD for variable stars lying in the field of NGC 7380.  $JHK$  data have been taken from 2MASS catalogue (Cutri et al. 2003). The sequences for dwarfs (solid curve) and giants (long dashed curve) are from Bessell & Brett (1988). The dotted curve represents the locus of TTSs (Meyer et al. 1997). The small dashed lines represent the reddening vectors (Cohen et al. 1981). The crosses on the reddening vectors represent an increment of visual extinction of  $A_V = 5$  mag.

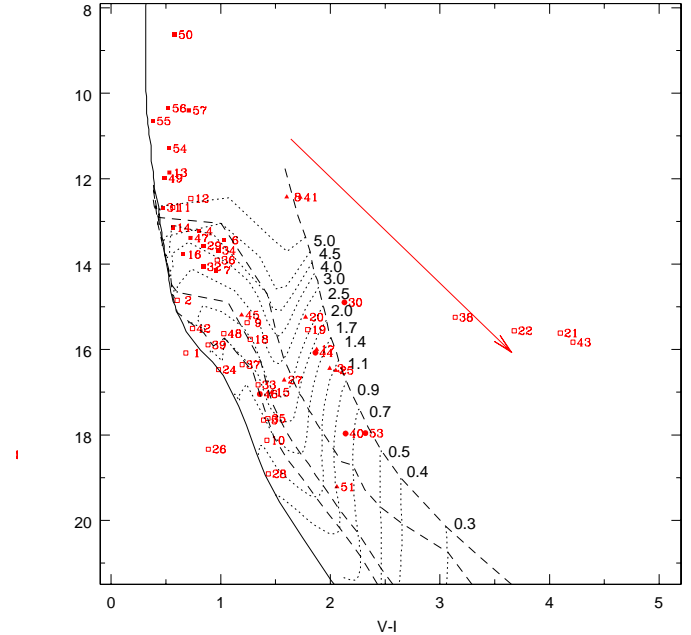


**Figure 7.**  $V/V-I$  colour-magnitude diagram of the cluster NGC 7380 for variable candidates. The filled circles and triangles represent probable CTTSs and WTTSs, respectively, whereas filled squares and open squares represent MS population in the cluster region and field population towards the cluster region, respectively. The ZAMS by Girardi et al. (2002) and PMS isochrones for 0.1, 1, 5, 10 Myrs by Siess et al. (2000) are shown. The dotted curves show PMS evolutionary tracks of stars of different masses. The isochores and evolutionary tracks are corrected for the cluster distance and  $E(V-I) = 0.625$  mag. The straight line indicates reddening vector for  $A_V/E(V-I) = 2.48$ .

tance  $< 2.6$  kpc and  $A_V \leq 1.55$  mag give the foreground contamination, and that with distance  $> 2.6$  kpc and  $A_V \geq 2.17$  mag give the background population. The advantage of this method is that we can separate the foreground (distance  $< 2.6$  kpc) and the background (distance  $> 2.6$  kpc) field star contamination. The fraction of contaminating stars upto  $V \sim 18$  has been determined as number of foreground and background stars (estimated from the model) over total number stars present in the observed cluster region (estimated from observed data) and it comes out to be 36%. Out of 57 variables studied here, 24 are found to be confirmed field star population which gives a contamination of about 42%, which is comparable with the model prediction.

#### 4 AGE AND MASS ESTIMATION

The age and mass of a PMS variable can be estimated with the help of PMS evolutionary tracks. The estimated ages of the majority of the YSOs are in the range of 0.1 to 5 Myr which are comparable to the ages of TTSs. The masses of the majority of PMS variables range from  $\sim 0.6$  to  $\sim 2.30 M_{\odot}$ . The associated errors in determination of age and mass can be of two kinds; random errors in observations and systematic errors due to the use of different theoretical evolutionary tracks. We have estimated the effect of random

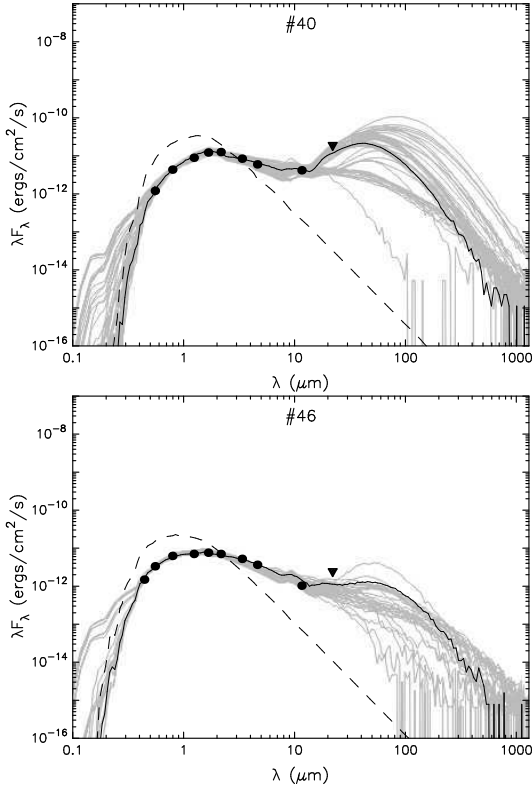


**Figure 8.** SEDs of the YSOs ID 40 and ID 46. The black line shows the best fit model, and the grey lines show subsequent models that satisfy  $\chi^2 - \chi_{\min}^2 \leq 2N_{\text{data}}$  criteria. The dashed line shows the stellar photosphere corresponding to the central source of the best fitting model. The circles denote the observed flux values. The triangle represents 22  $\mu\text{m}$  flux which is considered as upper limit while fitting.

errors in determination of age and mass by propagating the random errors to the observed estimations of  $V$ ,  $V - I$  and  $E(V - I)$  by assuming normal error distribution and using the Monte Carlo simulations (see e.g., Chauhan et al. 2009). Since we have used model by Siess et al. (2000) only for all the PMS stars, present age and mass estimations are not affected by the systematic errors. The presence of binaries may be another source of errors. The presence of binary will brighten a star, consequently yielding a younger age. In the case of equal mass binary, we expect an error of  $\sim 50$  to  $60\%$  in age estimation of the PMS stars. However, it is difficult to estimate the influence of binaries on mean age estimation as the fraction of binaries is not known. The estimated ages and masses along with their errors are given in Table 5.

## 5 SPECTRAL ENERGY DISTRIBUTION

To characterize the probable YSO variables further we have analyzed the spectral energy distribution of these sources using the radiative transfer models by Robitaille et al. (2006, 2007). Interpreting SEDs using the radiative transfer code is subject to degeneracy, however spatially resolved multiwavelength observations can reduce the degeneracy. We compiled the data of the YSOs at optical ( $BVI$ ; present work), NIR ( $JHK$ ; 2MASS survey), and WISE (3.4, 4.6, 12.0, and 22.0  $\mu\text{m}$ ; Cutri et al. 2012) bands, wherever available. We used

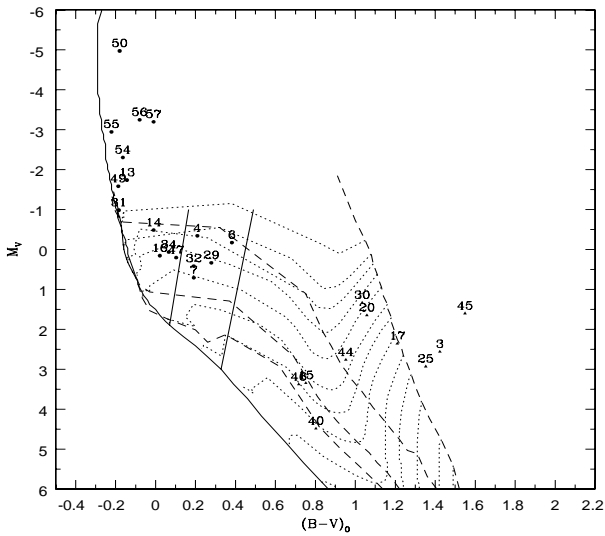
22  $\mu\text{m}$  data as upper-limit owing to its large beam ( $\sim 22$  arcsec) and crowded nature of the field. While fitting models we scaled the SED models to the distance of the cluster (i.e.,  $2.6 \pm 0.4$  kpc) and allowed a maximum  $A_V$  value determined by tracing back the YSOs current location on  $J/J - H$  diagram to the intrinsic dwarf locus along the reddening vector (see e.g., Samal et al. 2010), where the minimum extinction adopted as 1.5 mag, which is the foreground extinction towards the direction of cluster.

Fig. 8 shows the SEDs of two sources as examples. The WISE data were not available for the stars 15 and 45. Due to lack of mid and far-infrared, and millimeter data points, it is quite apparent that the SED models show high degree of degeneracy; nonetheless, barring star 8 and 41 SEDs of majority sources indicate the presence of IR-excess emission, possibly emission from circumstellar disk. We found that the observed SEDs of two sources (IDs. 8 and 41) are not well constrained. These two sources are possibly diskless stars or other reddened stellar sources along the line of sight. It is not possible to characterize all the SED parameters from the models due to limited observational data points. However, as discussed by Robitaille et al. (2007), some of the parameters can still be constrained depending on the available fluxes. In the present study, the SED models between 1  $\mu\text{m}$  to 12  $\mu\text{m}$  represent the data fairly well, hence, the stellar parameters are expected to be better constrained. However, it is worth noting that precise determination of stellar parameters using SED models requires data from optical to millimeter bands. In Table 5, the mass and age estimated using the SED model are also tabulated. Since our SED models are highly degenerate, the best-fit model is unlikely to give an unique solution, the tabulated values are the weighted mean and standard deviation of the physical parameters obtained from the models that satisfy  $\chi^2 - \chi_{\min}^2 \leq 2N_{\text{data}}$  data weighted by  $e^{(-\chi^2/2)}$  of each model as done in Samal et al. (2012), where  $\chi_{\min}^2$  is the goodness-of-fit parameter for the best-fit model and  $N_{\text{data}}$  is the number of input observational data points. Table 5 indicates that age and mass estimation using the SED models are higher by about 1.5 times in comparison to age and mass estimates using the  $V/V - I$  CMD. The estimate could be considered reasonable because of various uncertainties involved in SED modeling and lack of longer-wavelength data points to fully sample our SED.

## 6 $M_V/(B - V)_0$ AND LUMINOSITY ( $L/L_\odot$ ) VS. EFFECTIVE TEMPERATURE ( $T_{\text{EFF}}$ ) DIAGRAM

The  $M_V/(B - V)_0$  CMD for the identified MS and PMS stars is shown in Fig. 9. The intrinsic  $(B - V)$  colours of MS stars have been determined using the Q-method as described by Gutiérrez-Moreno (1975). For PMS stars we have used the average reddening ( $E(B - V) = 0.5$  mag) of the region. Fig. 10 shows the  $\log(L/L_\odot)/\log T_{\text{eff}}$  diagram for the MS variables. The absolute magnitude  $M_V$  was converted to luminosity using the relations  $\log(L/L_\odot) = -0.4(M_{\text{bol}} - M_{\text{bol},\odot})$ , and  $M_{\text{bol}} = M_V + BC$ , where BC is the bolometric correction. The bolometric magnitude  $M_{\text{bol},\odot}$  for the Sun has been taken as 4.73 mag (Torres 2010). To determine BC and effective temperature  $T_{\text{eff}}$  we used the relations between  $T_{\text{eff}}$ -





**Figure 9.**  $M_V/(B - V)_0$  colour-magnitude diagram for the MS and PMS stars of the cluster NGC 7380. The ZAMS by Girardi et al. (2002) and PMS isochrones for 0.1, 1, 5, 10 Myrs by Siess et al. (2000) are shown. The dotted curves show PMS evolutionary tracks of stars of different masses. The theoretical instability strip of Cepheids is taken from the literature (see Zwintz & Weiss 2006).

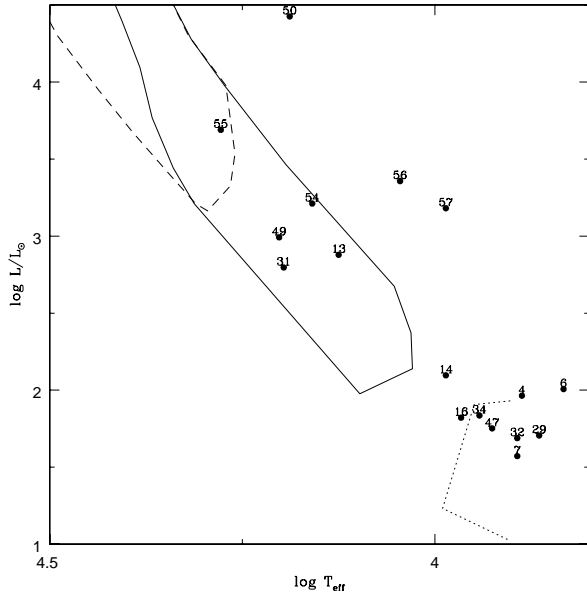


**Figure 10.**  $\log(L/L_\odot)/\log T_{eff}$  diagram for the probable MS variables towards the cluster NGC 7380. The theoretical SPB instability strip (continuous curve), empirical  $\delta$  Scuti instability strip (dotted curve) and the location of  $\beta$  Cep stars (dashed curve) are taken from the literature (see Balona et al. 2011; references therein).

**Table 4.** Classification of variable stars.

ID	$J - H/H - K$	$U - B/B - V$	$V/V - I$	Proper motion	X-ray	classification
1	no	-	no	-	-	Field
2	no	no	no	-	-	Field
3	yes	-	yes	-	-	PMS/WTTS
4	yes	yes	yes	yes	-	MS
5	no	-	no	-	-	Field
6	yes	yes	yes	yes	-	MS
7	yes	yes	yes	no	yes	MS/Field
8	?	no	yes	yes	-	Field
9	no	no	no	-	-	Field
10	No	-	no	-	-	Field
11	no	no	no	yes	-	Field
12	no	no	no	yes	-	Field
13	yes	yes	yes	yes	yes	MS
14	yes	yes	yes	yes	-	MS
15	yes	-	ye	-	yes	PMS/WTTS
16	yes	yes	yes	-	-	MS
17	yes	-	yes	-	-	PMS/WTTS
18	no	no	no	-	-	Field
19	no	no	no	-	-	Field
20	yes	no	yes	-	-	PMS/WTTS
21	no	-	no	-	-	Field
22	no	-	no	-	-	Field
23	no	-	-	-	-	Field
24	no	no	no	-	-	Field
25	no	-	yes	-	-	PMS/WTTS
26	no	-	no	-	-	Field
27	yes	-	yes	-	yes	PMS/WTTS
28	no	-	no	-	-	Field
29	yes	yes	yes	no	-	MS/Field
30	yes	yes	yes	yes	yes	PMS/CTTS
31	yes	yes	yes	yes	-	MS
32	yes	yes	yes	no	-	MS/Field
33	no	-	no	-	-	Field
34	yes	yes	yes	no	-	MS
35	no	-	no	-	-	Field
36	no	no	no	yes	-	Field
37	no	-	no	-	-	Field
38	no	-	no	-	-	Field
39	no	no	no	-	-	Field
40	yes	-	yes	-	-	PMS/CTTS
41	?	no	yes	yes	-	Field
42	no	no	no	-	-	Field
43	no	-	no	-	-	Field
44	yes	-	yes	-	-	PMS/WTTS
45	?	no	yes	-	-	PMS/WTT/Field
46	yes	-	yes	-	-	PMS/CTTS
47	yes	yes	yes	yes	-	MS
48	no	no	no	-	-	Field
49	yes	yes	yes	yes	-	MS
50	yes	yes	yes	yes	yes	MS
51	no	-	yes	-	-	PMS/WTTS
52	yes	-	-	-	-	PMS/WTTS
53	yes	-	yes	-	yes	PMS/CTTS
54	yes	yes	yes	yes	-	MS
55	yes	yes	yes	yes	-	MS
56	yes	yes	yes	-	-	MS
57	yes	yes	yes	-	-	MS

**Table 5.** Mass and age of probable PMS stars.

id	mass( $V/V - I$ ) $M_\odot$	age( $V/V - I$ ) Myr	mass(SED) $M_\odot$	age(SED) Myr
3	$1.17 \pm 0.13$	$0.25 \pm 0.02$	$3.262 \pm 0.467$	$0.533 \pm 0.120$
15	$1.92 \pm 0.16$	$4.55 \pm 2.06$	-	-
17	$1.58 \pm 0.11$	$0.26 \pm 0.03$	$3.112 \pm 0.472$	$0.627 \pm 0.201$
20	$2.36 \pm 0.15$	$0.23 \pm 0.03$	$3.011 \pm 0.006$	$1.193 \pm 0.006$
25	$1.07 \pm 0.06$	$0.22 \pm 0.05$	$2.356 \pm 0.245$	$0.401 \pm 0.135$
27	$2.16 \pm 0.06$	$1.60 \pm 0.46$	$2.188 \pm 0.254$	$2.086 \pm 1.067$
30	$2.06 \pm 0.08$	$0.10 \pm 0.01$	$6.164 \pm 0.021$	$0.262 \pm 0.004$
40	$0.78 \pm 0.08$	$0.59 \pm 0.06$	$1.622 \pm 1.055$	$0.523 \pm 0.434$
44	$1.58 \pm 0.11$	$0.28 \pm 0.03$	$2.377 \pm 0.754$	$0.485 \pm 0.164$
45	$2.28 \pm 0.09$	$4.22 \pm 0.57$	-	-
46	-	$> 5.00$	$1.816 \pm 0.249$	$4.885 \pm 1.005$
51	$0.73 \pm 0.36$	$4.00 \pm 4.47$	$1.135 \pm 0.373$	$4.965 \pm 2.976$
52	-	-	-	-
53	$0.62 \pm 0.05$	$0.32 \pm 0.19$	$3.421 \pm 0.850$	$0.107 \pm 0.053$

intrinsic  $(B - V)$  colours, and between  $T_{eff}$ -BC by Torres (2010). The luminosity ( $\log L/L_\odot$ ),  $M_{bol}$  and  $\log T_{eff}$  and BC of MS stars are listed in Table 6.

## 7 VARIABILITY CHARACTERISTICS

The sample phased light curves of identified MS, PMS and field population are shown in Figs. 11, 12 and 13 respec-

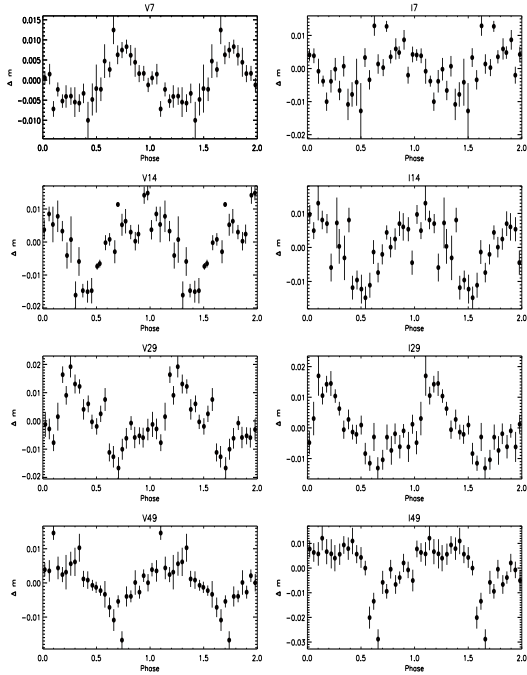


**Figure 11.** The sample phased light curves of MS variable stars in *V* and *I* bands. The complete figure is available electronic form only.

**Table 6.** The effective temperature ( $T_{eff}$ ), bolometric correction (BC), bolometric magnitude ( $M_{bol}$ ), luminosity ( $L$ ) and classification for MS stars.

ID	$\log T_{eff}$	BC	$M_{bol}$	$\log(L/L_{\odot})$	Classification
4	3.887	0.164	-0.179	1.964	$\delta$ Scuti or New Class
6	3.833	-0.113	-0.286	2.007	$\delta$ Scuti or New Class
7	3.893	0.0938	0.801	1.572	$\delta$ Scuti
13	4.125	-0.727	-2.465	2.879	SPB
14	3.986	-0.0234	-0.509	2.097	New Class
16	3.966	0.0234	0.177	1.822	$\delta$ Scuti or New Class
29	3.865	0.133	0.467	1.706	$\delta$ Scuti
31	4.196	-1.273	-2.258	2.796	SPB
32	3.893	0.094	0.510	1.689	$\delta$ Scuti
34	3.942	0.078	0.142	1.836	$\delta$ Scuti or New Class
47	3.926	0.148	0.351	1.752	$\delta$ Scuti
49	4.202	-1.164	-2.748	2.992	SPB
50	4.189	-1.359	-6.330	4.425	DHcep; Eclipsing binary
54	4.159	-0.992	-3.296	3.211	SPB
55	4.278	-1.547	-4.491	3.689	$\beta$ Cep
56	4.045	-0.414	-3.660	3.357	SPB
57	3.986	-0.023	-3.219	3.181	SPB

tively, where averaged differential magnitude in 0.04 phase bin along with  $\sigma$  error bars has been plotted. The phased light curves of all the MS, PMS and field variable stars are available online.

### 7.1 MS Variables of the cluster

Seventeen stars are found to be of MS type stars. The estimated periods of these stars range between 0.12d to 7.71d. The amplitudes of these variable stars are of a few mag. The location of the MS variables in the H-R diagram suggests that 4 stars (13, 31, 49 and 54) could be slow pulsating B (SPB) stars, whereas stars 7, 29, 32 and 47 could be  $\delta$  Scuti type stars. The location of star 14 is found to be between the

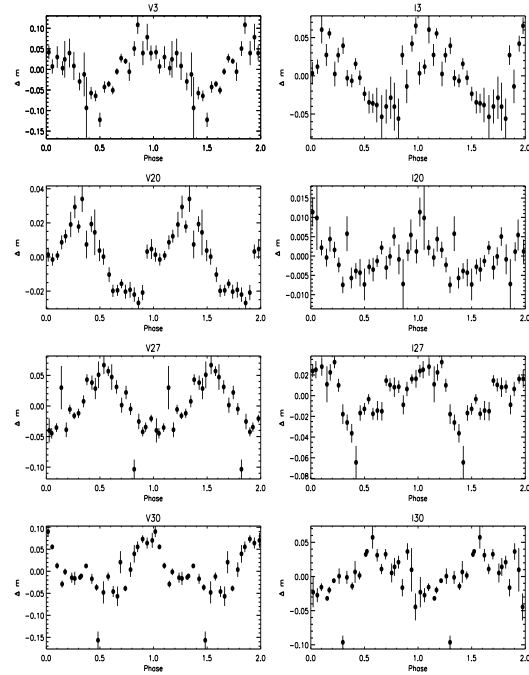


**Figure 12.** The sample phased light curves of PMS variable stars in *V* band and *I* bands. The complete figure is available electronic form only.

gap of SPB and  $\delta$  Scuti instability strip. Recently, Mowlavi et al. (2013) have found a large population of new variable stars between SPB stars and the  $\delta$  Scuti stars, the region where no pulsations were expected on the basis of theoretical models. Four stars namely 4, 6, 16 and 34 lie near the boundary of  $\delta$  Scuti instability strip. Star 55 could be  $\beta$  Cep type variable.

DH Cep (star no 50) = HD 215835 (R.A.=22h 46m 54.11s, Dec = +58° 05' 03.5", J2000) is the brightest star in the present sample and is considered to be the primary exciting star for the H II region S142. The star is a double-lined spectroscopic and eclipsing binary consisting of two very luminous O5/6 stars (Hilditch et al. 1996) close to the ZAMS. The binary star is an X-ray source, perhaps attributed to colliding winds (Pittard & Stevens 2002; Bhatt et al. 2010). The proper motion of DH Cep is estimated by Baumgardt et al. (2000) as  $\mu$  (RA),  $\mu$  (DEC) ( $-1.74 \pm 0.84$ ,  $-2.52 \pm 0.81$ ) mas yr $^{-1}$ , whereas the SHAO and UCAC3 values are found to be ( $-4.11 \pm 1.29$ ,  $-2.80 \pm 1.19$ ) mas yr $^{-1}$  and ( $-2.7$ ,  $-3.6$ ) mas yr $^{-1}$ , respectively. The measured radial velocity of DH Cep has been recorded as  $-33 \pm 2$  km/s (Hilditch et al. 1996),  $-35.4 \pm 1.8$  km/s (Pearce 1949), and  $-39 \pm 3$  km/s (Sturm & Simon 1994; Penny et al. 1997), which is consistent with it being part of the Perseus arm (Georgelin & Georgelin 1976). Our kinematic membership criterion for NGC 7380 region relies on the assumption that DH Cep is a member of the cluster. Our photometric observations of DH Cep reveals a period of 2.114 day which matches with earlier period determinations.

To characterize the variability of stars, in addition to the period, amplitude and shape of light curve of variable stars we need the location of variables in the H-R diagram. Fig. 10 show the H-R diagram for variables along with the

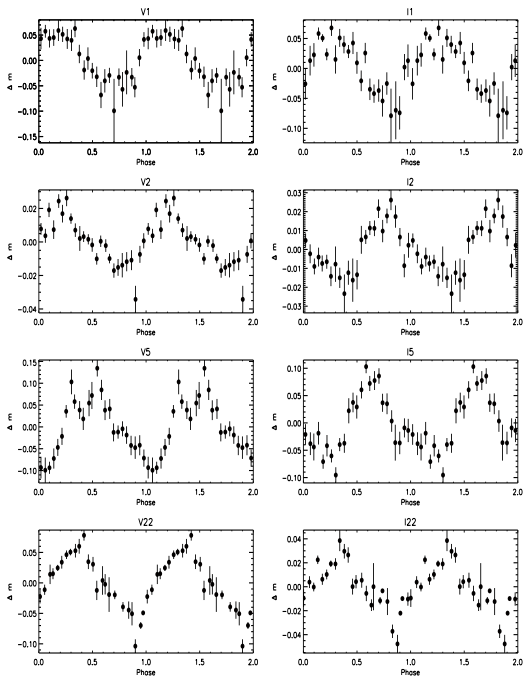


**Figure 13.** The sample phased light curves of field variable stars in  $V$  and  $I$  bands. The complete figure is available electronic form only.

theoretical SPB star instability strip, empirical  $\delta$  Scuti instability strip and the location of  $\beta$  Cep stars.

Underhill (1969) found that star 56 could be a foreground star of late A to F type, whereas star 57 could be an early B type star lying at the same distance as DH Cep. WEBDA on the basis of the photometric observations gives spectral type of star 57 as B0.5 V. Though these two stars 56 and 57 are located well away from the theoretical SPB strip in the H-R diagram, their variability characteristics suggest that these could SPB stars.

The spectral types of stars 54 and 55 is estimated by Underhill (1969) as B0.5 and B3 respectively, whereas WEBDA suggests the spectral types as B1V and B0.5V, respectively. Present photometric observations suggest the  $(B - V)_0$  colour of the stars 54 and 55 as -0.164 mag and -0.221 mag which indicate the photometric spectral types as B4.5V and B2.5V. The  $I$  band light curves of stars 54, 55, 56 and 57 suggest that these might be B type stars.

Photometric observations of stars 13, 31 and 49 also suggest that these could be B type MS stars. The spectral type of star 31 reported in WEBDA as B1.5 V. Their variability characteristics and location in the H-R diagram (cf Fig. 10) suggest that these could be SPB stars.

The stars 7, 29, 32 and 47 are located in the  $\delta$  Scuti instability region (cf Fig. 10). The variability characteristics of these stars also supports that these could be  $\delta$  Scuti stars. Star no 14 is located between the gap of SPB and  $\delta$  Scuti instability strip in the H-R diagram. Star numbered 4, 16 and 34 are lying near the boundary of the  $\delta$  Scuti instability strip; the periods of these stars are found to be 4.728 d, 0.406 d and 0.638d, respectively, which are longer than the reported periods of  $\delta$  Scuti stars (0.03d to 0.3 d). The amplitudes of these stars are in the range of 0.01 to 0.14 mag. The

period and amplitude of star 14 are 5.462 d and 0.014 mag. The proper motions (cf. Table 2) of 4, 14 and 34 suggest that these stars could be the member of cluster NGC 7380. We presume that the stars 4, 14, 16 and 34 could belong to new class of variable as suggested by Mowlavi et al. (2013).

## 7.2 PMS variables

The variations in the brightness of both WTTSs and CTTSs are found to occur at all wavelengths, from X-ray to infrared. The variability time-scale of TTSs ranges from a few minutes to years (Appenzeller & Mundt 1989). The variations in the brightness of TTSs are most probably due to the presence of cool or hot spots on stellar surface and circumstellar disk. The cool spots on the surface of the stars are produced by the emergence of stellar magnetic fields on the photosphere, and are thus indicators of magnetic activity. The cool spots on the photosphere rotate with stars hence are responsible for brightness variation in WTTSs. These WTTSs are found to be fast rotators as they have either thin or no circumstellar disk. The hot spots on the surface of young stars are the consequence of accretion process (Lynden-Bell & Pringle 1974; Koenigl 1991; Shu et al. 1994). Irregular or non-periodic variations are produced because of changes in the accretion rate. The time-scales of varying brightness range from hours to years. The accreting CTTSs show a complex behaviour in their optical and NIR light curves (Scholz et al. 2009).

The present sample consists of 14 probable PMS stars with 4 CTTSs and 10 WTTSs. The period of these PMS variables ranges from 0.13d to 53.64 d. The amplitude ranges from 0.008 to 0.371 mag. All of the CTTSs have longer periods ranging from 5.586 d to 53.644 d, whereas 5 WTTSs (out of 10) have periods less than 2 d. The amplitudes of CTTSs range from 0.05 mag to 0.37 mag, whereas most of the WTTSs in the present sample (7 out of the 10) have amplitudes less than 0.12 mag.

The larger amplitude in the case of CTTSs could be due to presence of hot spots on the stellar surface produced by accretion mechanism. Hot spots cover a small fraction of the stellar surface but with a high temperature causing larger amplitude of brightness variations (Carpenter et al. 2001). The smaller amplitude in WTTSs suggests dissipation of their circumstellar disks or these stars might have cool spots on their surface which are produced due to convection and differential rotation of star and magnetic field. This result is in agreement with that by Grankin et al. (2007, 2008) and by Lata et al. (2011, 2012).

## 7.3 Field population

The present sample contains 26 variables in the field. They have periods ranging from 0.05 d to 60.0 d which could belong to the field star population towards the direction of NGC 7380. The light curve of star 9 is similar to the RR Lyrae type variables. RR Lyrae variables pulsate with a period in the range between 0.2 and 1 day. RR Lyrae variables are old, low-mass pulsating stars. The characteristics of star 5 (period  $\sim$  0.32d, amp  $\sim$  0.12 mag) and 9 (period  $\sim$  0.26d, amp  $\sim$  0.08 mag) are consistent with being RR Lyrae variables. Stars 21, 22, 35, 38, 39, 42, 43 and 48 have periods greater than 10 days.

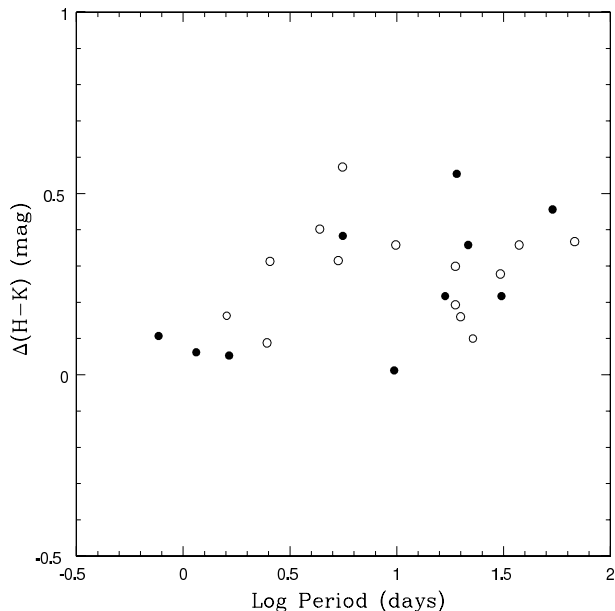


**Figure 14.** Rotation period vs  $\Delta(H - K)$ . The filled and open circles represent data for NGC 7380 and NGC 1893 clusters, respectively.

## 8 CORRELATION BETWEEN ROTATION AND $\Delta(H - K)$

A relation has already been found between the IR excess and the rotation rate for young stars. For example, Rebull et al. (2014) have found the IR excess does not necessarily imply longer periods, but a star with a longer period is more likely than those with shorter periods to have an IR excess. It is suggested that long period stars with little or no IR excess may have just recently cleared their disks and have not yet spun up in response to contraction on their way to the ZAMS. The NIR excess (e.g.,  $(H - K)$  excess) is a useful indicator for the presence of disk, hence can be used to look for the correlation between rotation and the presence/ absence of accretion disks. Here we define a parameter  $\Delta(H - K)$  as the horizontal displacement from the left reddening vector of ‘F’ region in the NIR-CC diagram of identified YSOs as shown in Fig. 6 assuming that  $\Delta(H - K)$  indicates NIR excess. Fig. 14 plots the relationship between  $\Delta(H - K)$  and rotation period of the YSOs. The data points for NGC 7380 are shown with filled circles whereas open circles represents data points for the young cluster NGC 1893 taken from our earlier work (Lata et al. 2014; Pandey et al. 2014). The variables having rotation period  $\leq 0.5$  d have not been included in the Fig. 14. There seems to be a correlation between NIR excess and period in the sense that YSOs having higher NIR excess, i.e., having disk, exhibit a longer rotation period. There seems to be a sudden change in the  $\Delta(H - K)$  at  $\log P \sim 0.4$  i.e.  $\sim 2.5$  d.

## 9 CORRELATION AMONG ROTATION, MASS, AGE, AND AMPLITUDE

To understand the correlation between mass/age of the TTSs and the rotation period we plot rotation period as a function of mass and age in Fig. 15. To increase the sam-

ple we have also included data for Be 59 from Lata et al. (2011) and NGC 1893 from Lata et al. (2012) because these clusters have similar environments, and moreover the same technique has been used to identify variable stars and to determine their physical properties. We have considered only those stars which have rotation period  $> 0.5$  d because rotation periods shorter than about 0.5 d would result in rotational velocities likely exceeding the break-up speed of T Tauri stars. Although there is a large scatter, the stars having masses  $\gtrsim 2 M_{\odot}$  ( $\log M/M_{\odot} = 0.3$ ) are found to be fast rotators. Similarly, the stars having ages  $\gtrsim 3$  Myr also seem to be fast rotators. This result is compatible with the disc locking model in which it is expected that stars with disc rotate slowly than those without (Edwards et al. 1993; Herbst et al. 2000; Littlefair et al. 2005). Fig. 16 plots amplitude of TTSs variability as a function of mass/ age of the YSO which, though with large scattering, reveals that amplitude of TTSs variability is correlated with the mass (left panel) and age (right panel) in the sense that amplitude decreases with increase in mass as well as age of a variable star. Deviations of individual sources of Be 59 and NGC 1893 have already been discussed in our earlier works (Lata et al. 2011, 2012). The decrease in amplitude could be due to the dispersal of the disk. Present result further supports our previous studies (Be 59: Lata et al. 2011; NGC 1893: Lata et al. 2012) that the disk dispersal mechanism is less efficient for relatively low mass stars. Right panel of Fig. 16 suggests that significant amount of the disks is dispersed by  $\lesssim 5$  Myr. This result is in accordance with the result obtained by Haisch et al. (2001).

## 10 SUMMARY

This work presents 57 variable stars in the cluster region of the NGC 7380. This study contains 14 PMS stars. The ages and masses of the majority of these PMS sources are found to be  $\lesssim 5$  Myr and in the range  $0.60 \lesssim M/M_{\odot} \lesssim 2.30$ , respectively and hence these could be T-Tauri stars. Four and 10 PMS stars are classified as CTTs and WTTs respectively. The periods of these PMS variables range from 0.13 d to 53.64 d. The amplitudes range from 0.008 mag to 0.371 mag. In addition we have found 17 MS variable stars (SPB stars,  $\delta$  scuti,  $\beta$  Cep and new class variable stars) and 26 variable stars belonging to the field star population. These are categorized on the basis of CMDs and TCDs. Variability characterisation has been done on the basis of period, amplitude, shape of light curves and location on the H-R diagram.

## 11 ACKNOWLEDGMENT

The authors are very grateful to the anonymous referee for a critical reading of the paper and useful comments. This study makes use of data products from the Wide-field Infrared Survey Explorer, which is a joint project of the University of California, Los Angeles, and the Jet Propulsion Laboratory/California Institute of Technology, funded by the National Aeronautics and Space Administration.

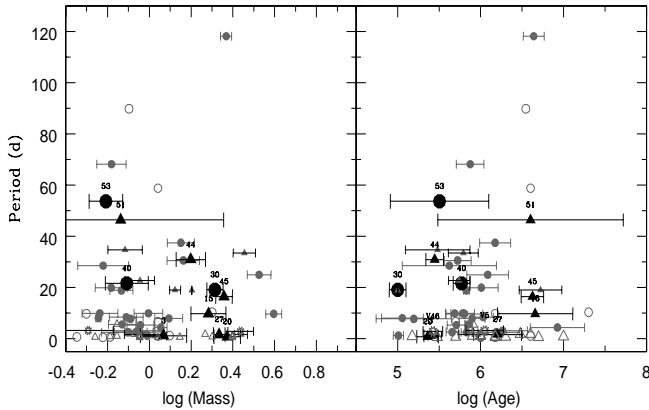


**Figure 15.** Rotation period of TTSs as a function of mass and age. Filled circles (larger; CTTs) and triangles (larger; WTTs) represent present data. Open and filled circles (CTTs), and open, filled triangles (WTTs) and starred circles (probable YSOs in NGC 1893) represent data for Be 59 and NGC 1893 taken from Lata et. al. (2011, 2012).

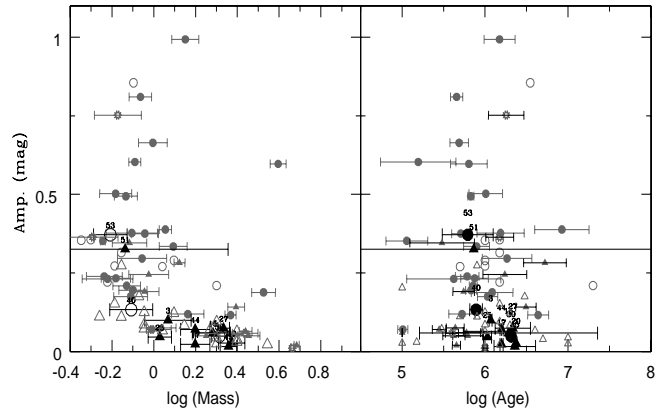


**Figure 16.** Amplitude of TTSs as a function of mass and age. Filled circles (larger; CTTs) and triangles (larger; WTTs) represent present data. Open and filled circles (CTTs), and open, filled triangles (WTTs) and starred circles (probable YSOs in NGC 1893) represent data for Be 59 and NGC 1893 taken from Lata et. al. (2011, 2012).

## REFERENCES

- [ ] Appenzeller I., Mundt R., 1989, A&AR, 1, 291
- [ ] Baade D., 1983, A&AS, 51, 235
- [ ] Balona L. A., Pigulski A., Cat P. De, Handler G., Gutiérrez-Soto J., Engelbrecht C. A., Frescura F., Briquet M., et al., 2011, MNRAS, 413, 2403
- [ ] Baumgardt H., Dettbarn C., Wielen R., 2000, A&AS, 146, 251
- [ ] Bessell M. S., Brett J. M., 1988, PASP, 100, 1134
- [ ] Bhatt H., Pandey J. C., Kumar B., Sagar R., Singh K. P., 2010, 15, 755
- [ ] Bhatt H., Pandey J. C., Singh K. P., Sagar R., Kumar B., 2013, JApA, 34, 393
- [ ] Bouvier J., Cabrit S., Fernandez M., Martin E. L., Matthews J. M., 1993, A&AS, 101, 485
- [ ] Bouvier J., 1994, in Caillault J.-P., ed., ASP Conf. Ser. Vol. 64, Cool Stars, Stellar Systems, and the Sun. Astron. Soc. Pac., San Francisco, p. 151
- [ ] Carpenter J. M., Hillenbrand L. A., Skrutskie M. F., 2001, AJ, 121, 3160
- [ ] Chauhan N., Pandey A. K., Ogura K., Ojha D. K., Bhatt B. C., Ghosh S. K., Rawat P. S., 2009, MNRAS, 396, 964
- [ ] Chen W. P., Pandey A. K., Sharma S., Chen C. W., Chen Li, Sperauskas J., Ogura K., Chuang R. J., Boyle R. P., 2011, AJ, 142, 71
- [ ] Cohen J. G., Persson S. E., Elias J. H., Frogel J. A., 1981, ApJ, 249, 481
- [ ] Crowther P. A., 2007, A&AR, 45, 177
- [ ] Cutri R. M., et al., 2012, Vizier Online Data Catalog, 2311, 0
- [ ] Cutri R. M., Skrutskie M. F., van Dyk S., Beichman C. A., Carpenter J. M., Chester T., Cambresy L., Evans T., Fowler J., Gizis J., et al., 2003, 2MASS All Sky Catalog of point sources
- [ ] Edwards S., Strom S. E., Hartigan P., Strom K. M., Hillenbrand L. A., Herbst W., Attridge J., Merrill K. M., Probst R., Gatley I., 1993, AJ, 106, 372
- [ ] Georgelin Y. M., Georgelin Y. P., 1976, A&A, 49, 57
- [ ] Girardi L., Bertelli G., Bressan A., Chiosi C., Groenewegen M. A. T., Marigo P., Salasnich B., Weiss A., 2002, A&A, 391, 195
- [ ] Grankin K. N., Melnikov S. Yu., Bouvier J., Herbst W., Shevchenko V. S., 2007, A&A, 461, 183
- [ ] Grankin K. N., Bouvier J., Herbst W., Melnikov S. Y., 2008, A&A, 479, 827
- [ ] Güdel M., Guinan E. F., Skinner S. L., ApJ, 1997, 483, 947
- [ ] Güdel M., 2004, A&A Rev., 12, 71
- [ ] Gutiérrez-Moreno A., 1975, PASP, 87, 805
- [ ] Haisch K. E., Lada E. A., Lada C. J., 2001, ApJ, 553, L153
- [ ] Herbst W., Herbst D. K., Grossman E. J., Weinstein D., 1994, AJ, 108, 1906
- [ ] Herbst W., Maley J. A., Williams E. C., 2000, AJ, 120,

- 349
- [ ] Hilditch R. W., Harries T. J., Bell S. A., 1996, *A&A*, 314, 165
  - [ ] Hillenbrand L. A., 2002, preprint (astro-ph/0210520)
  - [ ] Kiriakidis M., El Eid M. F., Glatzel W., 1992, *MNRAS*, 255, 1
  - [ ] Koenigl A., 1991, *ApJ*, 370, 39
  - [ ] Kudritzki R. P., Puls J., 2000, *ARA&A*, 38, 613
  - [ ] Lata S., Pandey A. K., Maheswar G., Mondal S., Kumar B., 2011, *MNRAS*, 418, 1346
  - [ ] Lata S., Pandey A. K., Chen W. P., Maheswar G., Chauhan N., 2012, *MNRAS*, 427, 1449
  - [ ] Lata S., Yadav Ram Kesh, Pandey A. K., Richichi A., Eswaraiah C., Kumar B., Kappelmann N., Sharma S., 2014, *MNRAS*, 442, 273
  - [ ] Lines H. C., Lines R. D., Guinan E. F., Robinson C. R., 1986, *IBVS*, 2932, 1
  - [ ] Littlefair S. P., Naylor T., Burningham B., Jeffries R. D., 2005, *MNRAS*, 358, 341
  - [ ] Lomb N. R., 1976, *ApSS*, 39, 447
  - [ ] Lucy L. B., White R. L., 1980, *ApJ*, 241, 300
  - [ ] Lynden-Bell D., Pringle J. E., 1974, *MNRAS*, 168, 603
  - [ ] Mathew B., Subramaniam A., Bhavya B., 2010, *BASI*, 38, 35
  - [ ] Mathew B., Banerjee D. P. K., Ashok N. M., Subramaniam A., Bhavya B., Joshi V., 2012, *RAA*, 12, 167
  - [ ] Meyer M. R., Calvet N., Hillenbrand L. A., 1997, *AJ*, 114, 288
  - [ ] Moffat A. F. J., 1971, *A&A*, 13, 30
  - [ ] Moskalik P., Dziembowski W. A., 1992, *A&A*, 256, 5
  - [ ] Mowlavi N., Barblan F., Saesen S., Eyer L., 2013, *A&A*, 554, 108
  - [ ] Owocki S. P., Cohen D. H., 1999, *ApJ*, 520, 833
  - [ ] Pandey A. K., Samal M. R., Yadav R. K., Richichi A., Lata S., Pandey J. C., Ojha D. K., Chen W. P., 2014, *NewA*, 29, 18
  - [ ] Pearce J. A., 1949, *AJ*, 54, 135
  - [ ] Penny L. R., Gies D. R., Bagnuolo William G., Jr., 1997, *ApJ*, 483, 439
  - [ ] Percy J. R., Gryc W. K., Wong J., Herbst W., 2006, *PASP*, 118, 1390
  - [ ] Percy J. R., Grynko S., Seneviratne R., Herbst W., 2010, *PASP*, 122, 753
  - [ ] Pittard J. M., Stevens I. R., 2002, *A&A*, 388, 20
  - [ ] Rebull L. M., Cody A. M., Covey K. R., et al., 2014, *AJ*, 148, 92
  - [ ] Robitaille T. P., Whitney B. A., Indebetouw R., Wood K., 2007, *ApJS*, 169, 328
  - [ ] Robitaille T. P., Whitney B. A., Indebetouw R., Wood K., Denzmore P., 2006, *ApJS*, 167, 256
  - [ ] Samal M. R., Pandey A. K., Ojha D. K., et al., 2012, *ApJ*, 755, 20
  - [ ] Samal M. R., Pandey A. K., Ojha D. K., et al., 2010, *ApJ*, 714, 1015
  - [ ] Scargle J. D., 1982, *ApJ*, 263, 835
  - [ ] Schaefer B. E., 1983, *ApJ*, 266, 45
  - [ ] Scholz A., Eisffel J., Mundt R., 2009, *MNRAS*, 400, 548
  - [ ] Semeniuk I., 1991, *IBVS*, 3656, 1
  - [ ] Shu F. H., Najita J., Ruden S. P., Lizano S., 1994, *ApJ*, 429, 797
  - [ ] Siess L., Dufour E., Forestini M., 2000, *A&A*, 358, 593
  - [ ] Stankov A., Handler G., 2005, *ApJS*, 158, 193
  - [ ] Stetson P. B., 1987, *PASP*, 99, 191
  - [ ] Stetson P. B., 1992, *J. R. Astron. Soc. Can.*, 86, 71
  - [ ] Strüder L., Briel U., Dennerl K., Hartmann R., Kendziorra E., et al., 2001, *A&A*, 365, 18
  - [ ] Sturm E., Simon K. P., 1994, *A&A*, 282, 93
  - [ ] Torres G., 2010, *AJ*, 140, 1158
  - [ ] Turner M. J. L., Abbey A., Arnaud M., Balasini M., et al., 2001, *A&A*, 365, 27
  - [ ] Underhill A. B., 1969, *A&A*, 1, 356
  - [ ] Vaiana G. S., Cassinelli J. P., Fabbiano G., Giacconi R., et al., 1981, *ApJ*, 245, 163
  - [ ] Zwintz K., Weiss W. W., 2006, *A&A*, 457, 237